JOC The Journal of Organic Chemistry

Article

pubs.acs.org/joc

Mechanism and Stereoselectivity of Biologically Important Oxygenation Reactions of the 7-Dehydrocholesterol Radical

Ramanan Rajeev and Raghavan B. Sunoj*

Department of Chemistry, Indian Institute of Technology Bombay, Powai, Mumbai 400076, India

Supporting Information

ABSTRACT: The mechanism of free radical oxygenation of 7-dehydrocholesterol (7-DHC), one of the biologically important sterols, is investigated by using density functional theory. The energetic origin of the product distribution and the stereoelectronic factors involved in various mechanistic pathways are delineated. The addition of triplet molecular oxygen to two types of conjugatively stabilized radicals, generated by the removal of the reactive allylic hydrogens from C9 or C14 positions, respectively denoted as H9 and H14 pathways, is studied. The *distortion–interaction analysis* of the C–O bond formation transition states suggests that the energetic preference toward the α prochiral face stems from reduced skeletal distortions of the cholesterol backbone as compared to that in the corresponding β prochiral face. This insight derived through a detailed quantitative analysis of the stereocontrolling transition states suggests that the commonly found interpretations solely based on steric interactions between the incoming oxygen and the protruding angular methyl groups (C10, C13 methyls) in the β face calls for adequate refinement. The relative energies of the transition states for molecular oxygen addition to C9, C5, and C14 (where spin densities are higher) and the ensuing products thereof are in agreement with the experimentally reported distribution of oxygenated 7-DHCs.

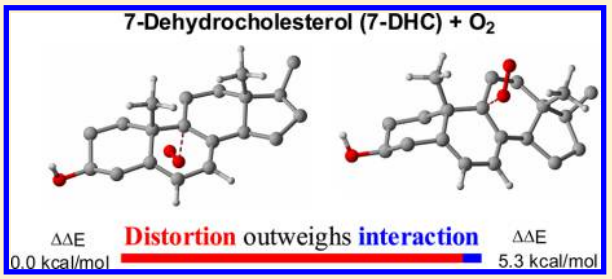

INTRODUCTION

The studies on the action of reactive oxygen species (ROS) on biological targets have been an active area of research for several decades now.[1] Oxidizable sterols such as cholesterol are important molecules that participate in oxidative stress regulatory mechanisms in living organisms. The free radical oxidation of sterols has been suggested to play vital roles in common diseases such as atherosclerosis and other neurodegenerative disorders.[2] The resulting oxysterol derivatives have been proposed to exhibit several deleterious effects including cytotoxicity.[3] One very important sterol that has received considerable recent attention is 7-dehydrocholesterol (7-DHC), a common biosynthetic precursor to cholesterol and vitamin D_3.[4] The reactions of 7-DHC are particularly important due to its (a) high reactivity toward molecular oxygen and (b) known connection with a metabolic disorder known as Smith–Lemli–Opitz syndrome (SLOS).[5] Higher levels of 7-DHCs and increased propensity for formation of oxysterols are noticed in individuals with SLOS disorder.

The primary starting point in these oxygenation reactions is the generation of sterol radicals by hydrogen abstraction.[6] Pioneering contributions from the Porter group have helped in understanding several sterol oxygenation reactions, including that of 7-DHC.[7] In a very recent study, Porter and co-workers have established the product distribution of several oxysterols obtained through the free radical chain oxidation of 7-DHC. The major oxygenated products are shown in Scheme 1.[8]

While the suggested mechanism has been effective toward rationalizing the observed product distribution, quantitative molecular-level insights have not been established yet. Herein we intend to disclose (a) the key features of the potential energy surfaces for the oxygenation of the 7-DHC radical, (b) the kinetic and thermodynamic factors responsible for the product selectivity in oxysterol formation, and (c) the stereoelectronic origin of the energetics.

RESULTS AND DISCUSSION

The energetic origin and the stereoelectronic factors that control the product distribution and regioselectivity in the oxygenation of the 7-DHC radical are presented in this article. The conventional atom numbering scheme, as shown in Scheme 2, is adopted. Two of the angular methyl groups at C10 and C13 are in β orientation while the hydrogens at the C9 and C14 ring junctions are α with respect to the steroidal framework.[9] The action of a radical initiator on parent 7-DHC can provide two conjugatively stabilized radicals as the major species, when the reactive allylic hydrogen atom is abstracted from C9 or C14. Herein, we focus on the energetic preferences for the reactions between these radicals with ground-state triplet molecular oxygen. The oxygenation products emanating from C9 and C14 radicals are respectively denoted as H9- and H14- mechanistic pathways.

The oxygen molecule can approach either from the α or the β face of the steroidal framework to form a bond with C9 or C5 (in the H9 mechanism). The spin density contour map of the

Received: April 19, 2013
Published: June 25, 2013

dx.doi.org/10.1021/jo4008496 | J. Org. Chem. 2013, 78, 7023–7029

Scheme 1. Major Products of Oxygenation of the 7-DHC Radical Followed by Reduction (ref 8)

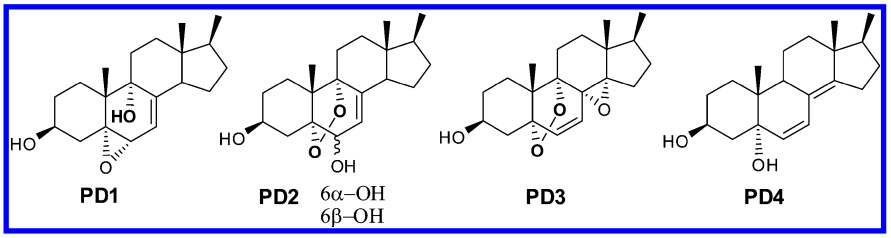

Scheme 2. H9 Pathway for the Addition of Oxygen to the 7-DHC Radical[a]

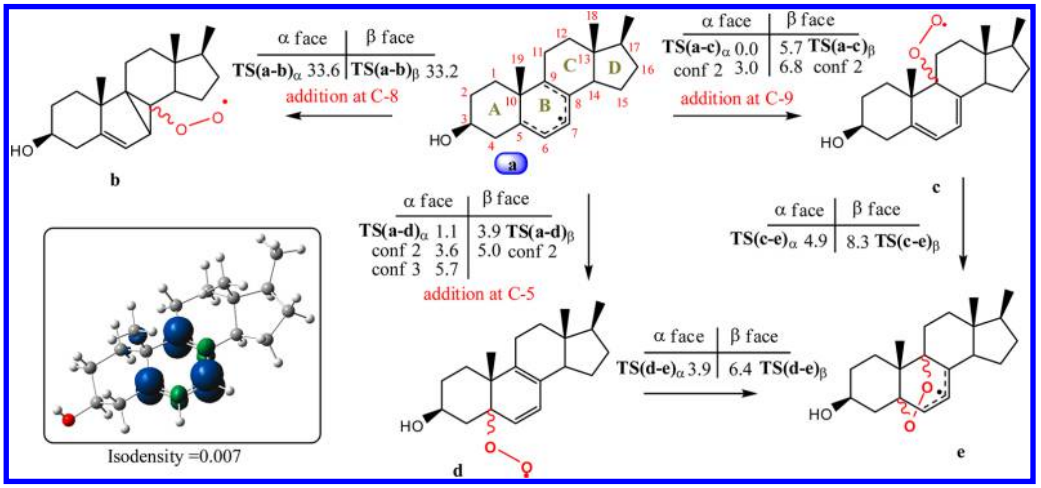

[a]The relative Gibbs free energies (in kcal/mol) are defined with respect to the lowest energy transition state at the UM06-2X/6-31+G** level of theory. The higher energy conformers of the transition states in each mode of addition are denoted as conf 2, conf 3, etc.

7-DHC radical (**a**) expressed as the difference in α and β spins, as shown in Scheme 2, indicates relatively higher spin densities at C9 and C5 sites, implying a ground-state propensity for additions at these two carbon centers. Three important branching pathways, depending on the site of attack of the incoming molecular oxygen on the B ring, can be envisaged (Scheme 2). The β face approach is expected to be of higher energy owing to the steric strain between the angular methyl groups and the incoming oxygen molecule.

The relative Gibbs free energies of the transition states for the C–O bond formation, calculated with respect to the lowest energy transition state, are summarized in Scheme 2. The addition of oxygen on the α prochiral face of the C9 radical center through **TS(a-c)**$_\alpha$ is the most preferred mode. Similarly, the addition at C5 via **TS(a-d)**$_\alpha$ is quite favored as well. Both C9 and C5 are conjugatively stabilized tertiary radicals. However, the corresponding additions on the β prochiral face, both at C9 and C5, are of much higher energy. The preference for the α prochiral face remained the same for some of the alternative conformers of these transition states (denoted by conf 1, conf 2, etc.) that differ in the relative orientation of the incoming oxygen molecule with respect to the developing C–O bond. Comparison of the energies of **TS(a-c)**$_\alpha$ and **TS(a-d)**$_\alpha$ further indicates a modest regioselectivity in favor of addition at the C9 position.

An alternative possibility involving the addition of oxygen at the C8 position is also examined. Conspicuously, the resulting peroxyl intermediate with a disrupted conjugation leads to transition states **TS(a-b)**$_{\alpha/\beta}$ as high as 33 kcal/mol compared that for **TS(a-c)**$_\alpha$. This prediction suggests that an extended conjugation in the peroxyl intermediate formed upon the initial addition of oxygen is one of the control elements dictating the ensuing product distribution. Furthermore, no products arising from C8 addition were identified in the experiments reported by Porter and co-workers.[8] Emphasis of our mechanistic study has therefore been placed on the pathways emerging from C9 and C14 addition of oxygen. In view of the significant spin density on C7, another possibility involving the addition of oxygen at C7 is additionally examined. Even though the initial C–O bond formation transition states are of lower energies, further cyclization of the peroxo radical with C9 and C5 positions through the α prochiral face is respectively 18 and 22 kcal/mol, which is much higher than that of other pathways considered in this study.[10] Similarly, the diastereomeric transition states for the corresponding cyclization through the β face are also of higher energy (19.2 and 22.1 kcal/mol, respectively, for C9 and C5 cyclization). However, energies of transition states for the initial bond formation comparable with other lower energy transition states can be viewed, similar to that for the oxygenation of linoleate.[7d] Geometries of the optimized transition states are included in Figure 1.

A careful analysis of the geometries of the lower energy diastereomeric transition state pairs, **TS(a-c)**$_\alpha$ and **TS(a-c)**$_\beta$, respectively, for the approach of the oxygen molecule through the α and β prochiral faces of the C9 radical center, reveals that C9–O1 and O1–O2 bond distances as well as the angle of approach of the oxygen molecule remain virtually the same in both of these TSs (Figure 1). Such close similarity in the vital geometric parameters is an indication of nearly identical electronic and molecular orbital interactions in these diastereomeric transition states. More importantly, the origin of the energy difference that controls the regio- and stereochemical preferences of 7-DHC oxygenation should therefore be regarded as arising due to the differences in the

dx.doi.org/10.1021/jo4008496 | J. Org. Chem. 2013, 78, 7023–7029

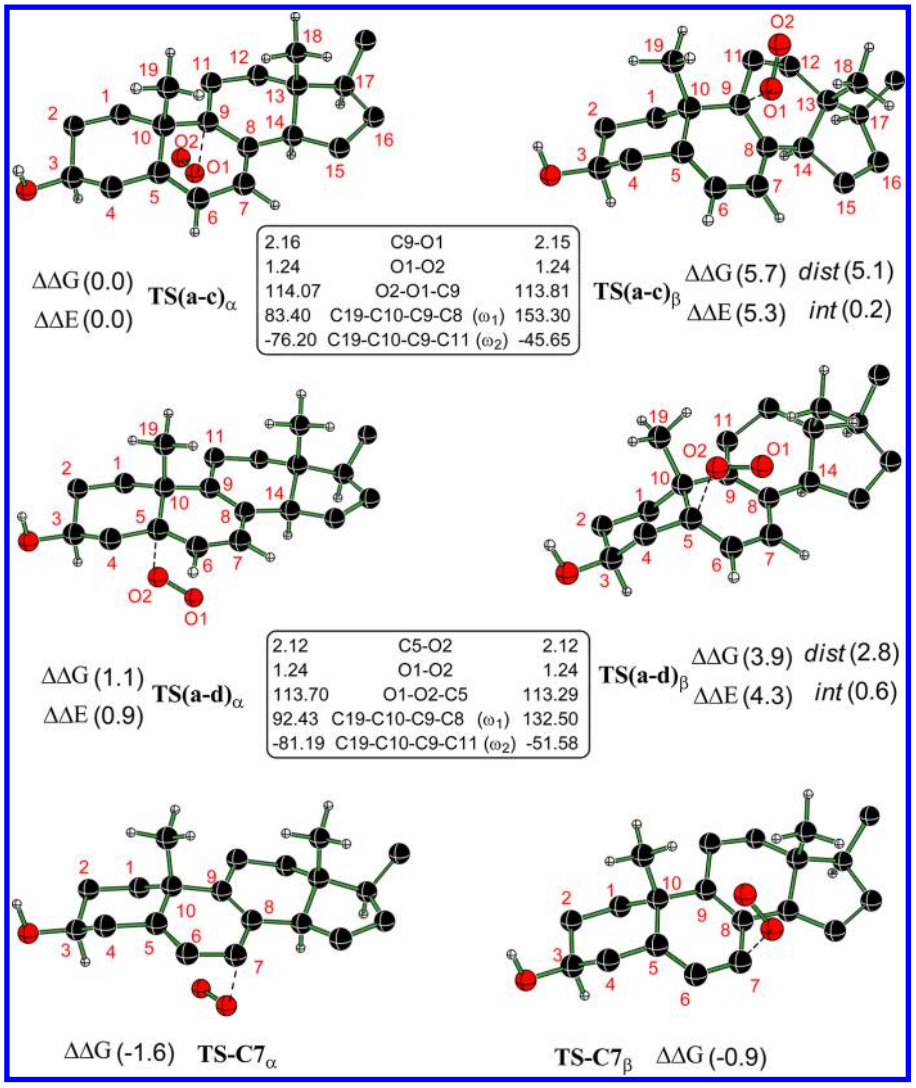

Figure 1. The optimized geometries of the transition states at the UM06-2X/6-31+G** level of theory for the H9 oxygenation pathway of the 7-DHC radical. Relative Gibbs free energies (ΔΔ*G*), relative energies (ΔΔ*E*), and the contributions due to *distortion* and *interaction* to ΔΔ*E* are given in kcal/mol. Atom colors: black (C), ivory (H), and red (O). (Distances are given in angstroms and angles in degrees).

skeletal geometric distortions. The dihedral angles such as ω_1 (C19−C10−C9−C8 dihedral angle) and ω_2 (C19−C10−C9−C11) capture the distortion in the A−B ring system in the transition state. In the lowest energy transition state **TS(a-c)**$_\alpha$, ω_1 and ω_2 are respectively 83.4° and −76.2° while those for **TS(a-c)**$_\beta$ are 153.3° and −45.6°. Corresponding values of ω_1 and ω_2 in the parent 7-DHC radical (**a**) are respectively 99.9° and −73.6°.[11] The cumulative effect of these distortions imparts increased strain to the fused rings and results in higher energy for **TS(a-c)**$_\beta$. To further quantify the molecular origin of the stereochemical preferences and the trends in the relative energies of the transition states involved in various pathways, *distortion−interaction analysis* of the transition states has been performed.[13]

In accordance with the distortion interaction model for transition states, the activation barrier is partitioned into the sum of destabilizing distortions within each reactant and stabilizing interactions between the reacting partners.[12] It is important to note that all distortion and interaction energies are based on total electronic energies (*E*). The discussions of distortion analysis are presented using ΔΔ*E* while those of kinetic and thermodynamic preferences employ the difference in Gibbs free energy (ΔΔ*G*). The distortion energy of the 7-DHC radical at the transition state geometry as a result of the approach of the oxygen is estimated. The origin of the electronic energy difference of 5.3 kcal/mol between **TS(a-c)**$_\alpha$ and **TS(a-c)**$_\beta$ is identified as arising due to higher distortion on the order of 5.1 kcal/mol and lower interaction by 0.2 kcal/mol in the latter transition state (Figure 1). The role of interaction between the oxygen molecule and the 7-DHC radical has only a little influence in controlling the relative energies of the diastereomeric transition states. The stereochemical preference for the α face approach can therefore be attributed to a reduced skeletal distortion emanating from the B ring in **TS(a-c)**$_\alpha$.

Next, cyclization of the peroxyl radicals (**c** and **d**) to form an endoperoxy allyl radical intermediate (**e**) is examined. The transition state **TS(d-e)**$_\alpha$ for the cyclization of the C5 peroxy radical is lower in energy as compared to that for the C9 peroxyl intermediate. Again, the ring closure of the α peroxyl intermediate is favored over that of the corresponding β analogue. Radical **e** can now undergo either a fragmentation to an oxyepoxy radical (**m**) or react with another molecule of oxygen (vide infra). Interestingly, one of the major products noticed by Porter and co-workers is a hydroxyl epoxide, which

dx.doi.org/10.1021/jo4008496 | J. Org. Chem. 2013, 78, 7023−7029

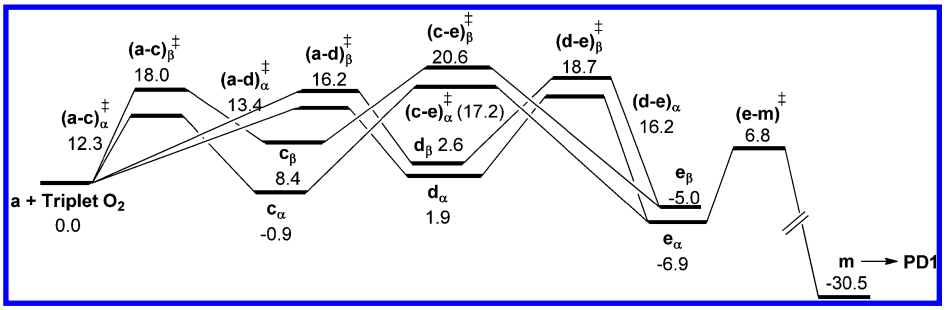

Figure 2. Gibbs free energy profile for the formation of endoperoxy allyl radical **m**. Free energies (in kcal/mol) are obtained at the UM06-2X/6-31+G** level of theory.

Scheme 3. Fragmentation of Intermediate e and the Addition of a Second Molecule of Oxygen

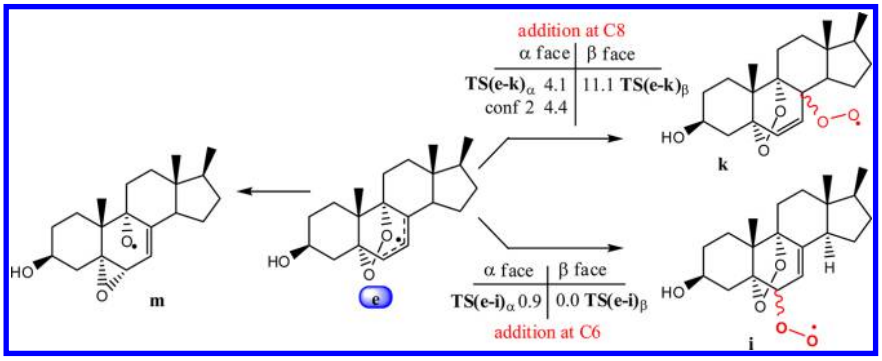

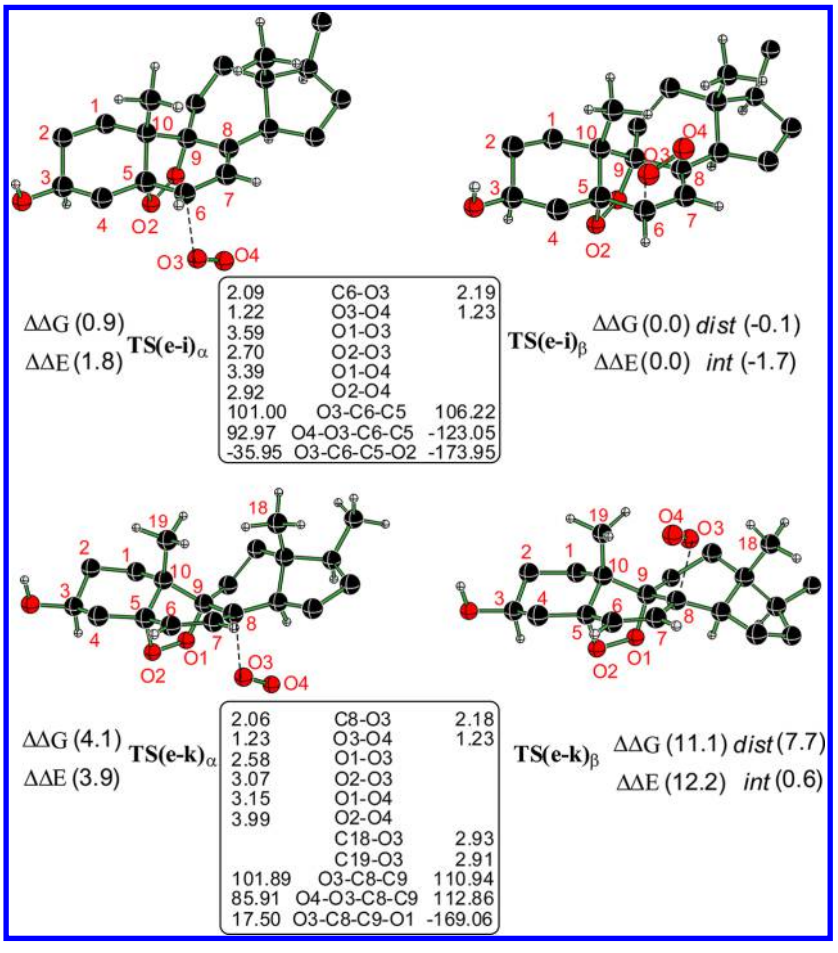

Figure 3. The optimized geometries of the transition states at the UM06-2X/6-31+G** level of theory for the addition of a second molecule of oxygen to endoperoxy allyl radical **e**. All other descriptions are the same as those in Figure 1.

dx.doi.org/10.1021/jo4008496 | J. Org. Chem. 2013, 78, 7023−7029

can be readily obtained through a hydrogen atom transfer to radical **m**. The other major products of oxygenation of the 7-DHC radical followed by reduction in a span of 24−32 h of reaction time is shown in Scheme 1. Two interesting patterns are evident: (a) products **PD1**, **PD3**, and **PD4** are formed by oxygen addition through the α face; (b) diminishing chiral discrimination at the C6 position results in both α and β **PD2** products.

From the Gibbs free energy profile (Figure 2) it is clear that the fragmentation of **e** is highly preferred. An exergonicity of −30.5 kcal/mol as well as a low-lying transition state with a relative energy of 6.8 kcal/mol with respect to the separated intermediate **a** and triplet oxygen molecule suggests a facile reaction. Hydrogen atom abstraction by radical **m** will directly yield **PD1**, which is one of the major products of oxygenation of the 7-DHC radical, in concert with a previous experimental observation.

In view of formation of multiply oxygenated products such as **PD2** and **PD3** in 7-DHC oxygenation, the addition of a second molecule of oxygen at both C8 and C6 positions of **e** is considered as shown in Scheme 3.[13] The bridged oxygens are identified to impart a pronounced effect in directing the incoming oxygen molecule, particularly at the C-6 position. Contrary to the α facial preference for the addition of the first oxygen molecule, the approach of the second oxygen molecule via the β face through **TS(e-i)**$_\beta$ is modestly more preferred (0.9 kcal/mol). In other words, the low energy separation between **TS(e-i)**$_\alpha$ and **TS(e-i)**$_\beta$ can be regarded as the origin of the lack of facial selectivity in the formation of **PD2** wherein both 6α-OH and 6β-OH are noticed. Similarly, identification of only one stereoisomer of **PD3** by the addition of oxygen through the α face is also evident from the computed energy difference of 7 kcal/mol between **TS(e-k)**$_\alpha$ and **TS(e-k)**$_\beta$.

The distortion−interaction analysis (Figure 3) conveys that the interaction energy between the reacting fragments are better in **TS(e-i)**$_\beta$ than in the diastereomeric **TS(e-i)**$_\alpha$. In the case of addition of oxygen at C8, the repulsion with the angular methyl groups are more pronounced than in C6 addition wherein the electrostatic repulsion between the bridging oxygen and the incoming oxygen is a dominant factor.

As described earlier, the generation of the 7-DHC radical can occur by hydrogen abstraction either from C9 or C14. Hitherto discussions have been on the reactions of the H9 pathway for the C9 radical. Similar scenarios for the addition of an oxygen molecule to the C14 radical center, known as the H-14 mechanism shown in Scheme 4, are also examined.[14] The Gibbs free energy difference between C14 and C5 addition is only 0.6 kcal/mol, indicating a diminished regiochemical preference as compared to that noted in the H9 mechanism.[15] However, the facial discrimination between α and β faces for the oxygen addition at the C5 radical center is quite prominent, as the Gibbs free energy difference between the diastereomeric transition states is about 5 kcal/mol. In the case of C14 addition, the corresponding energy difference is about 1.5 kcal/mol, again indicating a fairly good facial preference toward the α face addition.

Efforts to rationalize the relative energy ($\Delta\Delta E$) separation of 4.4 kcal/mol between **TS(p-q)**$_\alpha$ and **TS(p-q)**$_\beta$ by using the distortion−interaction method conveys some interesting trends. The total distortion of the 7-DHC radical and molecular oxygen accompanying the formation of a new C−O bond is lower in **TS(p-q)**$_\alpha$ by 6.5 kcal/mol for the α face addition as compared to that in **TS(p-q)**$_\beta$ for the β face addition (Figure 4). However, the favorable interaction energy between the oxygen molecule and the 7-DHC radical is weaker by 2.1 kcal/mol in **TS(p-q)**$_\alpha$.[16] The overall stabilization of 4.4 kcal/mol ($\Delta\Delta E$) enjoyed by **TS(p-q)**$_\alpha$ thus offers the crucial energy difference desirable for stereoselectivity. Stereoselectivity in the formation of **PD4** arises because of this appreciable energy difference. Thus, it is evident that a dominant distortion outweighs the effect of interaction in the case of the H14 pathway. Similar to that of the H9 pathway, the key to higher distortion in the β face addition is traced to the conformational distortion in B and C rings. The geometry of **TS(p-q)**$_\beta$ is more distorted than that of **TS(p-q)**$_\alpha$ (Figure 4). A structural distortion parameter such as ω_3 in the radical intermediate **p** and in the transition state **TS(p-q)**$_\alpha$ is respectively 66.1° and 66.3° while that in **TS(p-q)**$_\beta$ is 88.4°. Similarly, dihedral angle ω_4 is also characteristic of an increased skeletal distortion in **TS(p-q)**$_\beta$ for the β face addition. It is interesting to note at this juncture that improved interaction energy between the reacting partners in the transition state may not offer any direct kinetic advantage for the reaction to occur from the same prochiral face.

Scheme 4. Mechanism of Oxygen Addition to the C14 and C5 Radical Centers[a]

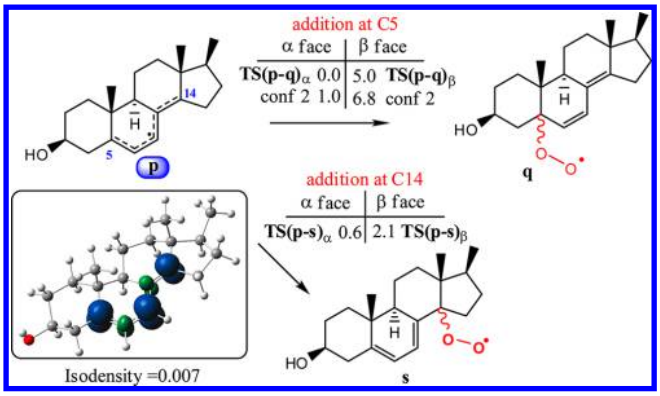

[a]For details of energies, see Scheme 2.

The discussions until now could rationalize the energetic factors controlling the formation of all major products **PD1** through **PD3**, as shown in Scheme 1. One of the most important aspects of the H14 mechanism is that the most preferred mode for oxygen addition is identified to be via **TS(p-q)**$_\alpha$ through the α face. This pathway would yield peroxyl radical **q**, which upon reduction and hydrogen atom transfer would provide **PD4**. Another possibility involving a hydrogen abstraction by intermediate **s** leading to the C14 hydroperoxide intermediate is also examined.[17] Mechanistic features are similar to those of the H-9 mechanism emanating from the C-9 radical.

CONCLUSIONS

The UM06-2X/6-31+G** density functional theory studies on the mechanism of oxygenation of the 7-DHC radical have been able to successfully rationalize the formation of the experimentally identified products formed in the oxygenation of the 7-DHC radical by triplet molecular oxygen. The majority of important oxygenated sterol formations can be rationalized by invoking the H9 mechanism (wherein the free radical is initially generated by the abstraction of the hydrogen atom from C9). The most preferred pathway has been computed to involve α face addition of molecular oxygen. The distortion of

dx.doi.org/10.1021/jo4008496 | J. Org. Chem. 2013, 78, 7023−7029

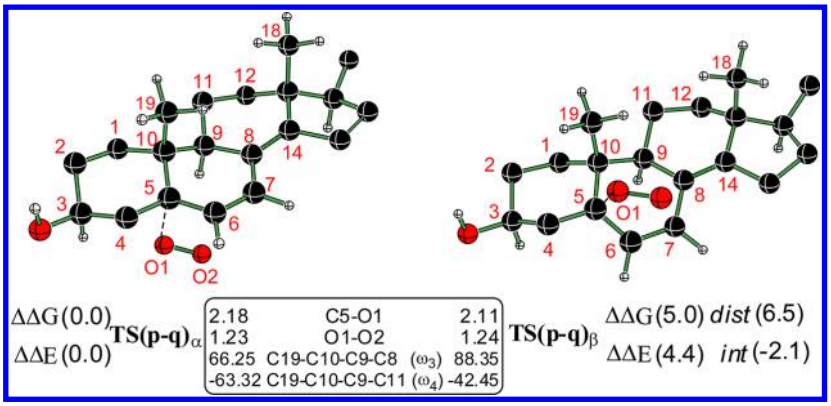

Figure 4. The optimized geometries of the transition states obtained at the UM06-2X/6-31+G** level of theory for the addition of oxygen to the C5 radical center involved in the H14 mechanism. Atom designations and details of energies are similar to those in Figure 1.

the skeleton rings in the transition states is identified as the origin of facial preference for the approach of molecular oxygen. The experimental observation that one of the major products, 6α- and 6β-hydroxy endoperoxides, are formed in nearly equal proportions is due to very low facial selectivity in the addition of a second molecule of oxygen to an endoperoxy radical. In an enzymatic reaction wherein the molecules react in a congested space, the role of distortion in the transition state should be carefully considered rather than relying entirely on interaction energies between the receptor and the reactive substrate(s) or between substrates.

COMPUTATIONAL METHODS

All the calculations were carried out using the Gaussian09 suite of quantum chemical programs.[18] Optimized geometries of different stationary points were characterized using the corresponding Hessian indices. All transition states were characterized as the first-order saddle points by harmonic vibrational frequency analysis. Wherever possible, intrinsic reaction coordinate (IRC) calculations were carried out to verify these transition states as connected to the reactants and products.[19] Additional geometry optimizations using more stringent criteria, such as opt=calcfc, as implemented in the electronic structure program, were carried out on the end points of IRC runs to connect these structures to the minimum energy product/reactant on either side of the transition state. The metahybrid density functional, UM06-2X, which captures dispersion interaction, was used as the primary computational method for geometry optimizations.[20] Pople's 6-31+G** basis set was employed for all calculations. A series of additional computational model chemistries, including higher order electron correlation at the UCCSD(T)/6-31G* level of theory were applied to a model system, and the results were compared with the UM06-2X/6-31+G** level of theory.[21] Spin contamination of the computed wave functions after spin annihilation fell within the range of 0.75 to 0.79.

Gibbs free energies were obtained by adding the thermal and entropic contributions to the gas-phase electronic energies at the UM06-2X/6-31+G** level of theory. Gibbs free energies in the gas phase are used for the discussions unless otherwise specified explicitly. The distortion−interaction analyses on the transition states were carried out by evaluating the interaction energies between the distorted reactants as noticed in the transition state geometry as well as the distortion energy within each of the reacting partners in the transition state geometry as compared to the respective undistorted reactants.[22] All distortion interaction energies are based on total electronic energies. As the cholesterol molecule possesses rigid trans-fused ring junctions, the conformational possibilities are primarily confined to different orientations of the incoming oxygen molecule with respect to the cholesterol framework. Different likely orientations of molecular oxygen were considered and are described at appropriate sections in the manuscript.

ASSOCIATED CONTENT

Supporting Information

Optimized geometries of all the stationary points, total electronic energies, and details of distortion−interaction analysis. This material is available free of charge via the Internet at http://pubs.acs.org.

AUTHOR INFORMATION

Corresponding Author

*E-mail: sunoj@chem.iitb.ac.in. Fax: 91 222 576 7173.

Notes

The authors declare no competing financial interest.

ACKNOWLEDGMENTS

Generous computing time from IIT Bombay computer center is gratefully acknowledged. R.R. acknowledges CSIR (New Delhi) for a Senior Research Fellowship. Financial support from the Industrial Research and Consultancy Centre (IRCC-IIT Bombay) for a research associate position is additionally acknowledged.

REFERENCES

(1) Jahn, U.; Galano, J. M.; Durand, T. *Angew. Chem., Int. Ed.* **2008**, *47*, 5894.

(2) (a) Esterbauer, H.; Gebicki, J.; Puhl, H.; Jurgens, G. *Free Radical Biol. Med.* **1992**, *13*, 341.

(3) Korade, Z.; Xu, L.; Shelton, R.; Porter, N. A. *J. Lipid Res.* **2010**, *51*, 3259.

(4) (a) Janowski, B. A.; Willy, P. J.; Devi, T. R.; Falck, J. R.; Mangelsdorf, D. J. *Nature* **1996**, *383*, 728. (b) Raoult, D.; Audic, S.; Robert, C.; Abergel, C.; Renesto, P.; Ogata, H.; Scola, B. L.; Suzan, M.; Claverie, J. M. *Science* **2004**, *306*, 1344. (c) Lang, M.; Murat, S.; Clark, A. G.; Gouppil, G.; Blais, C.; Matzkin, L. M.; Guittard, E.; Yanagawa, T. Y.; Kataoka, H.; Niwa, R.; Lafont, R.; Villemant, C. D.; Orgogozo, V. *Science* **2012**, *337*, 1658. (d) Shen, Y.; Wollam, J.; Magner, D.; Karalay, O.; Antebi, A. *Science* **2012**, *338*, 1472.

(5) (a) Yin, H.; Xu, L.Porter, N. A. *Chem. Rev.* **2011**, *111*, 5944 and the reference therein. (b) Korade, Z.; Xu, L.; Mirnics, K.; Porter, N. A. *J. Inherit. Metab. Dis.* **2013**, *36*, 113.

(6) Iuliano, L. *Chem. Phys. Lipids* **2011**, *164*, 457.

(7) (a) Porter, N. A. *Methods Enzymol.* **1984**, *105*, 273. (b) Porter, N. A. *Acc. Chem. Res.* **1986**, *19*, 262. (c) Porter, N. A.; Caldwell, S. E.; Mills, K. A. *Lipids* **1995**, *30*, 277. (d) Tallman, K. A.; Pratt, D. A.; Porter, N. A. *J. Am. Chem. Soc.* **2001**, *123*, 11827.

(8) Xu, L.; Korade, Z.; Porter, N. A. *J. Am. Chem. Soc.* **2010**, *132*, 2222.

(9) The hexyl side chain of C17 is replaced with a methyl group to minimize the computational complexities. The effect of the side chain

is expected to be minimal on the energetics of oxygen addition, as it remains away from the site of reaction.
(10) Relative free energies for this addition are −1.6 and −0.9 kcal/mol, respectively, for α and β face additions.
(11) Additionally, in **TS(a-c)**$_\alpha$, the C19 methyl group is relatively more staggered (−76°) with respect to C9-C11 bond than in **TS(a-c)**$_\beta$ (−45°).
(12) For further details of distortion−interaction analysis, see the computational methods given in Supporting Information.
(13) For C8 addition, in the case of the α face, O_2 can orient at a dihedral angle of −30° and 156° with respect to the C8−C14 bond to give product **k**. However, only one such possibility exists for the β facial approach. At C6 only one possible orientation is feasible on both face α and β faces.
(14) The difference in energies of radicals **a** and **p** is only 3 kcal/mol. Computed vertical bond dissociation energies (BDE) for the formation of C9, C14, and C4 radicals are respectively 99.8, 100.3, and 113.5 kcal/mol. The higher BDE for the C4 radical formation indicates that reactions ensuing from C4 radicals are quite unlikely.
(15) Similar to that in the C-9 mechanism, higher spin density at C-7 can be thought of as capable of leading to oxygen addition at the C7 position. Relative free energies of transition states are −0.5 and 0.4 kcal/mol for α and β face additions.
(16) (a) Molecular electrostatic potential of **TS(p-q)**$_\beta$ shows a favorable interaction between methyl hydrogens and the oxygen molecule (See Figure S1 in Supporting Information). The atoms-in-molecule (AIM) analysis identified a ring critical point (ρ_{rcp} = 0.015) between two of the methyl hydrogen atoms and one of the oxygen atoms of the incoming oxygen molecule. (b) Bader, R. F. W. *Atoms in Molecules: A Quantum Theory*; Clarendon Press: Oxford, 1990. (c) AIM2000 (Version 2.0), The Buro fur Innovative Software, SBK-Software, Bielefeld, Germany.
(17) Possible pathways from the C-9 radical of the C14 hydroperoxide intermediate **a′** are summarized in Scheme S1 in Supporting Information.
(18) Frisch, M. J., et al. *Gaussian 09 Revision A.02*; Gaussian, Inc., Wallingford, CT, 2004. The complete list of citations is provided in Supporting Information
(19) (a) Gonzalez, C.; Schlegel, H. B. *J. Chem. Phys.* **1989**, *90*, 2154. (b) Gonzalez, C.; Schlegel, H. B. *J. Phys. Chem.* **1990**, *94*, 5523.
(20) (a) Zhao, Y.; Truhlar, D. G. *J. Chem. Phys.* **2006**, *125*, 1. (b) Zhao, Y.; Truhlar, D. G. *Theor. Chem. Acc.* **2008**, *120*, 215.
(21) See Scheme S2 and Table S1 in Supporting Information.
(22) (a) Diefenbach, A.; Bickelhaupt, F. M. *J. Phys. Chem. A* **2004**, *108*, 8460. (b) Jong, G. T. D.; Visser, R.; Bickelhaupt, F. M. *J. Organomet. Chem.* **2006**, *691*, 4341. (c) Jong, G. T. D.; Bickelhaupt, F. M. *Chem. Phys. Chem.* **2007**, *8*, 1170. (d) Jong, G. T. D.; Bickelhaupt, F. M. *J. Chem. Theory Comput.* **2007**, *3*, 514. (e) Ess, D. H.; Houk, K. N. *J. Am. Chem. Soc.* **2007**, *129*, 10646. (f) Ess, D. H.; Houk, K. N. *J. Am. Chem. Soc.* **2008**, *130*, 10187. (g) Hayden, A. E.; Houk, K. N. *J. Am. Chem. Soc.* **2009**, *131*, 4084. (h) Shinisha, C. B.; Sunoj, R. B. *J. Am. Chem. Soc.* **2010**, *132*, 12319. (i) Rajeev, R.; Sunoj, R. B. *Org. Biomol. Chem.* **2011**, *9*, 2123. (j) Rajeev, R.; Sunoj, R. B. *J. Org. Chem.* **2012**, *77*, 2474.